Karlsruhe Institute of Technology

Atomic displacement cross-sections for neutron irradiation of materials based on arc-dpa and NRT models with JEFF-4, ENDF/B-VIII.1, JENDL-5, and TENDL-2023 data

A.Yu. Konobeyev, D. Leichtle

KIT SCIENTIFIC WORKING PAPERS 264

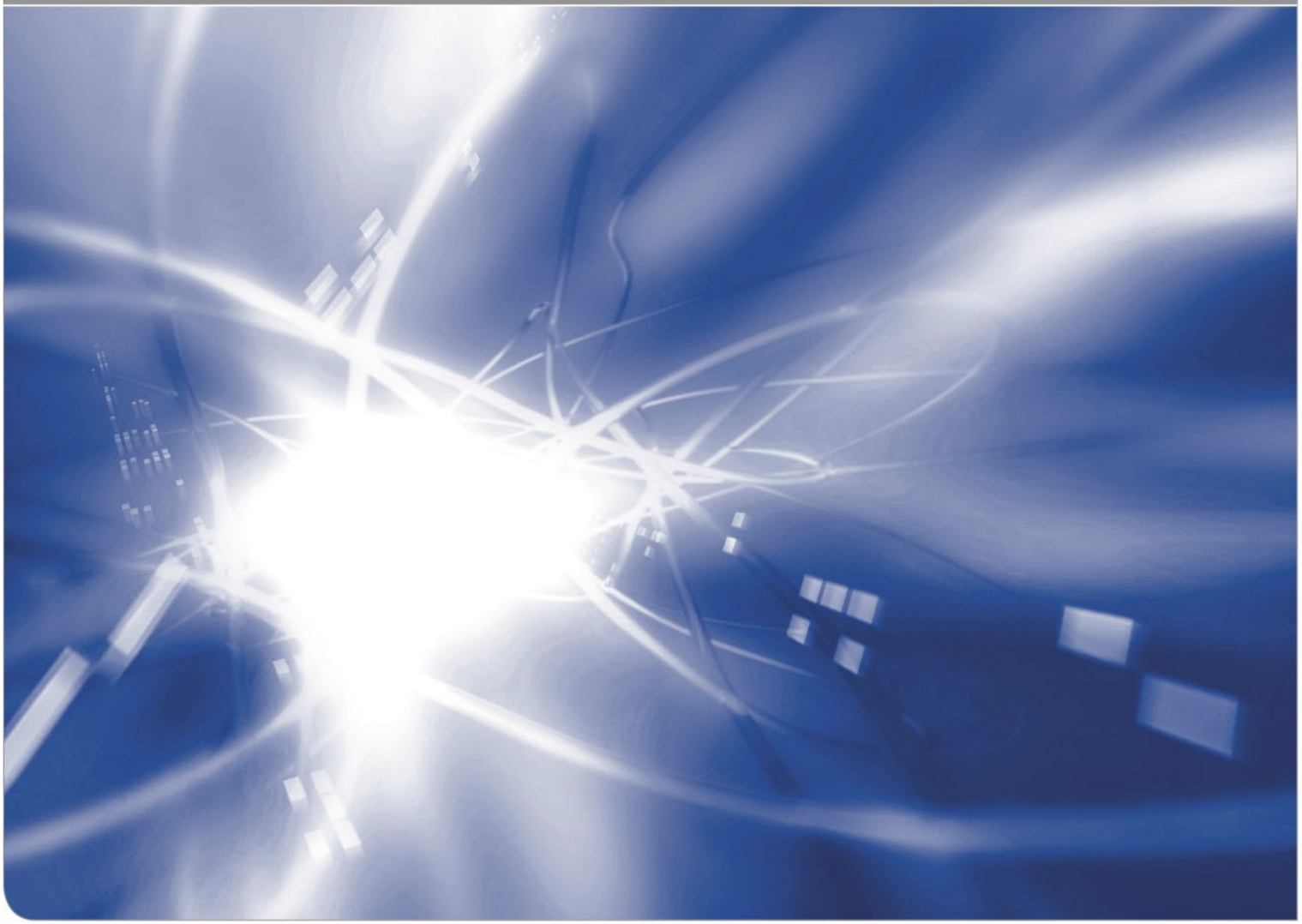

INR, Karlsruhe Institute of Technology, 76344 Eggenstein-Leopoldshafen, Germany

Impressum

Karlsruher Institut für Technologie (KIT)
www.kit.edu

2025

ISSN: 2194-1629

Abstract

Atomic displacement cross-sections for a detailed assessment of radiation damage rates were calculated for materials from lithium to bismuth using the arc-dpa and NRT models with data from the JEFF-4, ENDF/B-VIII.1, JENDL-5 (with updates through July 2024), and TENDL-2023 (August 2024) libraries over neutron energies from 10^{-5} eV to the highest available energies.

Where necessary, the cross-sections derived from each library were extended to 200 MeV using TENDL-2023 and earlier TENDL releases.

The displacement cross-sections obtained from JEFF-4 were provided with covariance matrices.

The prepared data in ENDF-6 and ACE formats, along with their accompanying illustrations, are available at:https://bwsyncandshare.kit.edu/s/83HW426X4XQEQwZ

CONTENTS

page

1. **Introduction** …… 1

2. **Tools and data used for the calculations** …… 2

2.1 Calculation of the number of stable defects produced by irradiation …… 2

2.1.1 Arc-dpa model …… 2

2.1.2 Joint arc-dpa-BCA or MD-BCA calculations …… 2

2.2 Nuclear data used …… 3

2.3 Processing data using the NJOY code …… 3

2.4 Displacement cross-section extension up to 200 MeV …… 5

2.5 Calculation of covariance matrices …… 7

3. **Displacement cross-sections** …… 8

3.1 Data from 10^{-5} eV up to maximum available energy in files …… 8

3.2 Data extended to 200 MeV …… 10

4. **Conclusion** …… 14

Acknowledgement …… 15

References …… 16

Appendix Defect generation efficiency calculated for beryllium, aluminium, iron, copper, and tungsten using various neutron spectra …… 21

1. Introduction

Seven years ago, atomic displacement cross-sections were obtained for a broad set of elements [1-4] using the arc-dpa [5] and NRT [6,7] models. The cross-sections were calculated using neutron data from then-current versions of nuclear data libraries ENDF/B-VIII.0 [8], JEFF-3.3 [9], JENDL-4 [10], and TENDL-2017 [11]. Four years later, the displacement cross-sections were updated [12] with newer datasets JEFF-4T1 [13], JENDL-5 [14], and TENDL-2021 [15]. With the recent release of updated versions of these nuclear data libraries, there is a renewed need to recalculate and refine the displacement cross-sections accordingly.

The present work aims to provide updated arc-dpa and NRT dpa cross-sections for elements ranging from lithium to bismuth. These calculations are based on the most recent data from the libraries JEFF-4.0 [16], ENDF/B-VIII.1 [17], JENDL-5 (with updates through July 2024) [18], and TENDL-2023 (August 2024 release) [19].

Arc-dpa model parameters were adopted from [5,20-22], with modifications as discussed in Ref. [12]. Unlike previous works [1-3,12], this study did not use results of joint modelling of arc-dpa and the binary collision approximation method (arc-dpa-BCA) or molecular dynamics (MD – BCA). The reasons for this are discussed below.

The nuclear recoil spectra were calculated using the NJOY code [23], version (2016.78), with the necessary modifications. The PREPRO-2023 code [24] and several service codes were applied to calculate displacement cross-sections for natural mixtures of isotopes and other auxiliary calculations.

Where necessary, the obtained displacement cross-sections were extended to primary neutron energies of up to 200 MeV using the TENDL-2023 library and earlier versions of the library. Details are discussed below.

Covariance matrices were added to the displacement cross-sections prepared using JEFF-4 data. The uncertainties and correlations of the cross-sections were evaluated as described in Refs.[25-27], and are discussed below. Uncertainties in both the nuclear data themselves and in the models used to calculate the number of displacements were considered.

The resulting displacement cross-sections were recorded in ENDF-6 and ACE formats.

Section 2 briefly describes the general details of the calculations. Section 3 presents the resulting cross-sections.

2. Tools and data used for the calculations

This section provides a brief overview of the models, data, and computer codes used to obtain the displacement cross-sections.

2.1 Calculation of the number of stable defects produced by irradiation

2.1.1 Arc-dpa model

The defect generation efficiency in the arc-dpa model is calculated as described in [5]. For most of the materials, the c_{arcdpa} parameters and E_d values were taken from Ref.[21]. The value of b_{arcdpa} was taken equal to -0.82 [27]. The notation used in [5] is retained in this work.

For beryllium b_{arcdpa}, c_{arcdpa}, and E_d values were taken from Ref.[22], for iron, nickel, copper, palladium, tungsten, and platinum from Nordlund and co-authors [5], and for silver and gold from Nordlund [20].

2.1.2 Joint arc-dpa-BCA or MD-BCA calculations

In a previous study [12], displacement cross-sections for beryllium, aluminum, iron, copper, and tungsten were calculated using defect production numbers obtained through a combined arc-dpa–BCA or MD-BCA approach [28]. In such calculations, ion-ion interactions were simulated using the BCA method until the kinetic energy of the moving ions dropped below a certain threshold energy T_{crit} [28]. Below this energy, the number of generated defects was estimated according to the arc-dpa model or the results of molecular dynamics simulations. Results from these calculations can be found, for example, in [2,28], and many other studies.

It should be noted that in the present work, as in Ref.[29], results from arc-dpa–BCA and MD-BCA modelling are not used. The reason is both the lack of necessity for this study and the relative uncertainty in determining the value of T_{crit}. For most reactor spectra - such as those considered in [30,31] - the displacement cross-sections integrated over the neutron spectrum show similar values when using defect numbers based solely on arc-dpa calculations compared to numbers obtained using

combined arc-dpa–BCA methods. However, for some types of spectra, the maximum discrepancies reach 30-50% for iron, copper, and tungsten. Detailed data on the average defect generation efficiency for various neutron spectra are given in the Appendix. Arc-dpa - BCA modelling was carried out using the IOTA code [28].

A characteristic feature of the defect generation efficiency (η) in arc-dpa–BCA and MD-BCA methods is its increase with rising energy of primary ions, starting from a certain primary ion energy.

The data of Dunlop et al. [32] for Fe–Fe and O–Fe were used in [2, 28] as indirect evidence for an increase of η with energy; see, for example, Figs. 1 and 2 in Ref. [2]. At the same time, as noted by Yin [33], the data from [32] used in [2,28] should be reduced by if one uses a more accurate value of the Frenkel pair resistivity than that presented in Ref. [32]. This suggests a possibly smoother increase of η with energy than that obtained in arc-dpa-BCA and MD–BCA simulations in Refs. [2,28].

Molecular dynamics simulations performed by [34] also indicate a possible increase in defect generation efficiency with increasing energy. Moreover, it seems doubtful that the measured high-energy displacement cross-sections, similar to those presented in Refs. [35–39], can be adequately described without using the arc-dpa–BCA or MD-BCA approach, while at the same time matching the defect generation efficiency obtained in the reactor experiments reported in Ref.[30], see also [31].

2.2 Nuclear data used

The nuclear data were taken from the following libraries:

- Final release of JEFF-4.0 [16],
- ENDF/B-VIII.1 [17],
- JENDL-5 (with updates through July 2024) [18],
- TENDL-2023 (August 2024) [19].

Processing was performed using NJOY (version 2016.78) [23] with the HEATR module, modified to perform calculations using the arc-dpa approach.

2.3 Processing data using the NJOY code

The HEATR module of NJOY was extended to enable the calculation of displacement cross-sections using the arc-dpa model and the results of arc-dpa–BCA or MD–BCA simulations, if necessary.

In addition, as noted by Simakov [40], the standard version of NJOY does not use the ASTM standard [41] for calculations based on the NRT model. The HEATR module has been updated to support such calculations, as well to vary NRT model parameters, which is necessary for estimating the uncertainty of displacement cross-sections calculated using the NRT model.

Input data for HEATR has been modified. New parameters, *carc*, *barc*, and *kwas*, have been added to the "read" instruction, which, among other things, inputs the value of E_d (*break*):

read(nsysi,) matd,npk,nqa,ntemp,local,iprint,break, carc, barc, kwas*

Carc and *barc* are parameters of the arc-dpa model. The parameter *kwas* can take the following values:

kwas = *-2* : default option, NRT model, usual processing. The sections MF=3, MT=444-447 contain *eV×barn* data
Not an ASTM standard. *Carc* und *barc* are not used.

kwas = *-1* : as *kwas*= *-2*, but the MT=444-447 contain displacement cross-sections in barn, i.e. the NRT multiplier $0.8/(2E_d)$ is included. Not the ASTM standard

kwas = *0* : The sections MF=3, MT=444-447 include displacement cross-sections in barn. The NRT model and the ASTM standard. *Carc* und *barc* are not used.

0 < *kwas* < 99 : arc-dpa displacement cross-sections (MT=444-447) in barns.
Default values for these parameters are not supported.
Break (E_d), *carc*, and *barc* must be entered.

kwas = *99* : The sections MT=444-447 contain displacement cross-sections in barn. The efficiency of the defect generation (N_D/N_{NRT}) is taken from a special file with a simple format.
The file name with the efficiency must be entered in the next line. *Carc*, *barc* are not used.

kwas = *100* : as *kwas* = *0*, but the three parameters for scaling the coefficients in the NRT formula are entered in the next line. See function DF of the code and Ref. [26].
The option is used to estimate the uncertainty in NRT based displacement cross-sections.

kwas = 777 : as *kwas = 99*, but the number of defects (N_D) for a principal ion (recoil, PKA) is taken from a special file.
The N_D data for other ions will be “scaled” using NRT.

The modified HEATR module is available upon request [42].

2.4 Displacement cross-section extension up to 200 MeV

The evaluated nuclear data libraries were extended up to 200 MeV for all materials whose original files had a maximum energy below this value. Such an extension was necessary for each of the following libraries: JEFF-4, ENDF/B-VIII.1, JENDL-5, and TENDL-2023.

In most cases, the extension was performed using data from TENDL-2023. For certain light materials, earlier versions of TENDL were employed, as specified in Table 1. These same versions were also used to extend displacement cross-sections derived from TENDL-2023 data.

Table 1. TENDL versions used to extend displacement cross-sections up to 200 MeV

Z	Target	TENDL version
3	Li^{6} and Li^{7}	2014
4	Be^{9}	2011
5	B^{10} and B^{11}	2011
6	C^{12}	2012
6	C^{13}	2021
7	N^{14} and N^{15}	2011
8	O^{16}	2011
8	O^{17} and O^{18}	2021
9	F	2010

Typically, the original data were retained up to the maximum energy available in the evaluated files. Exceptions were made for specific materials, including iron and tungsten, for which TENDL-2023 data were used starting from energies as low as 20–50 MeV. This decision was motivated by the good agreement observed between TENDL-2023 and displacement cross-sections calculated using various nuclear reaction models, in contrast to the discrepancies found between the original library data and those model-based calculations. Such calculations included the use of various versions of the intranuclear cascade model to calculate the nonelastic component of the displacement cross-sections [43] and the optical model [44,45] to calculate the elastic component.

Figures 1 and 2 show the NRT displacement cross-sections obtained for iron and tungsten using the JEFF-4 and TENDL-2023 libraries, as well as calculated values. The data shown in Figs. 1, 2 are also representative of the ENDF/B library.

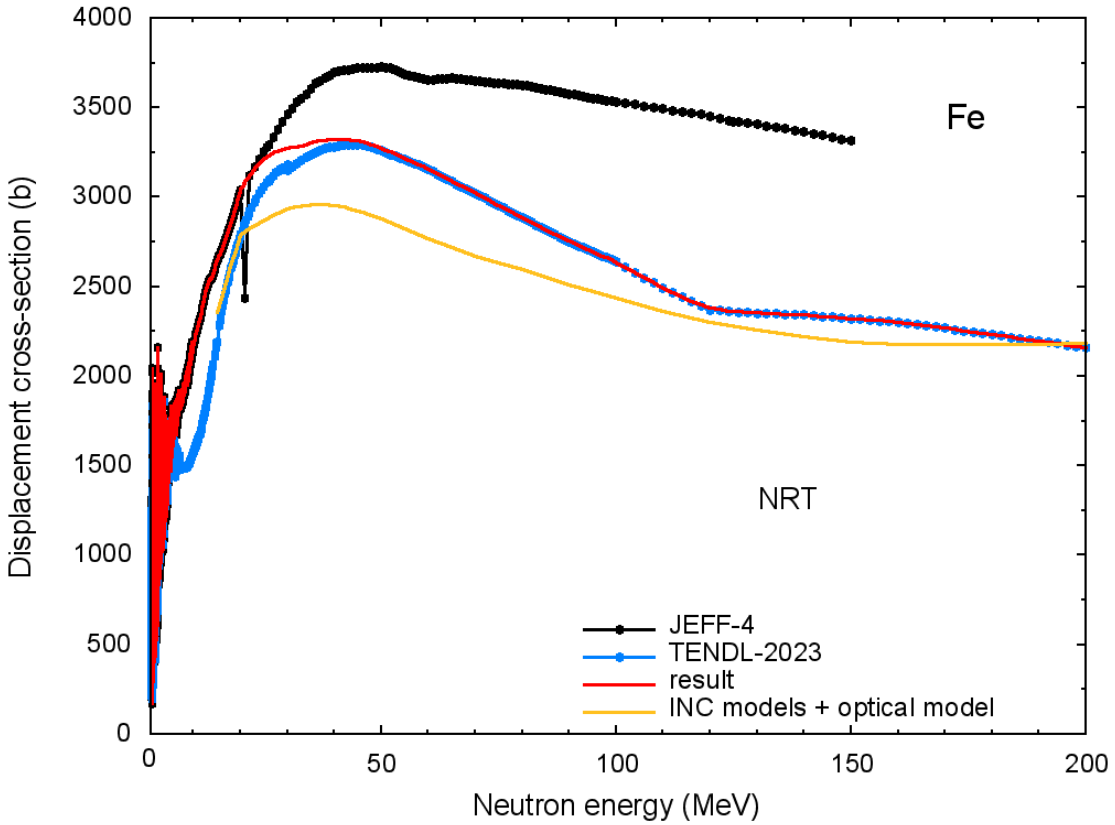

Fig.1 Extension of displacement cross-sections from JEFF-4 for iron up to 200 MeV. The curve labelled "*INC models + optical model*" correspond to the sum of the average displacement cross-section for nonelastic neutron interactions with the material - calculated using seven different modifications of the intranuclear cascade model - and the cross-section for elastic neutron scattering. The E_d value is equal to 40 eV.

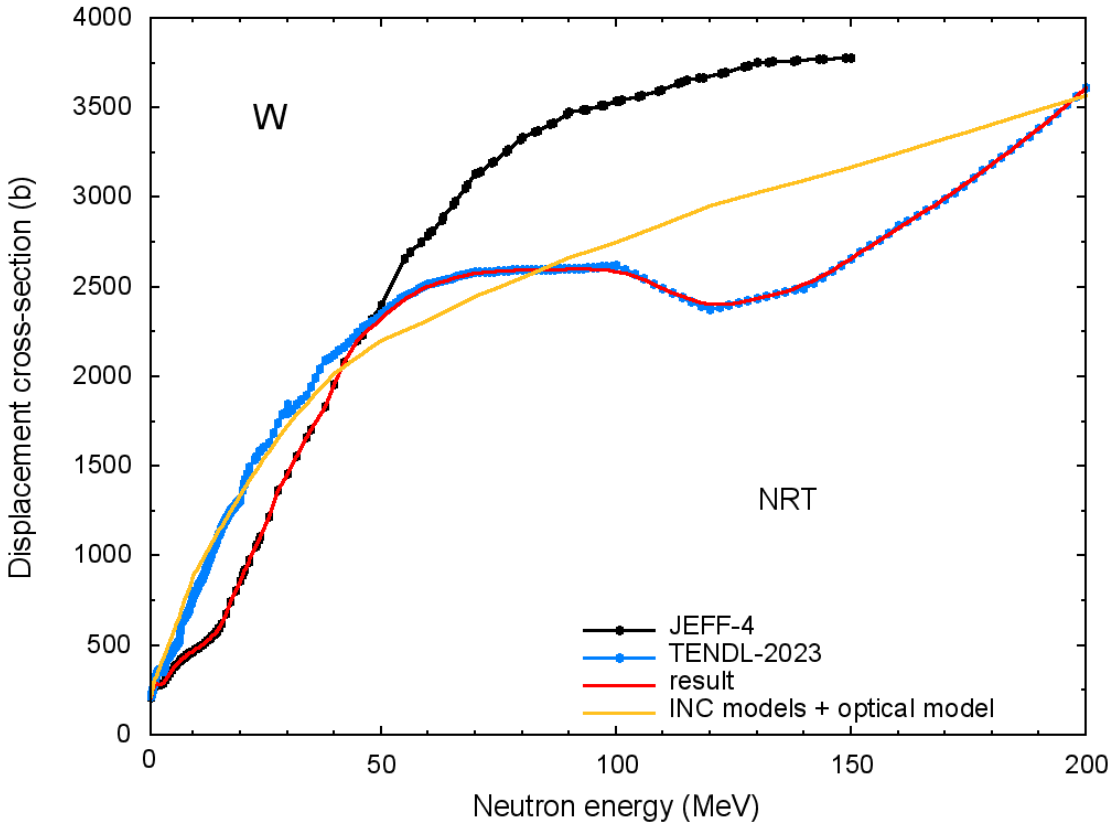

Fig.2 The same as in Fig. 1, but for tungsten. The E_d value is equal to 70 eV.

2.5 Calculation of covariance matrices

In this study, covariance matrices were obtained for arc-dpa and NRT displacement cross-sections calculated using JEFF-4. It was assumed [27] that the main source of uncertainty in the displacement cross-sections is the uncertainty in the total cross-sections and the parameters of models describing the number of generated defects. For NRT, the "internal" model uncertainty was taken into account, as explained in [26], rather than the differences between the NRT predictions and the results of arc-dpa or MD calculations — that is, not the type of uncertainty that would “cover” such differences.

The calculation of covariance matrices was carried out as follows:

- generation of random files taking into account the uncertainty of total cross-sections;
- Monte Carlo generation of *N* sets of input data for the NJOY version with additions, considering the variation in arc-dpa and NRT parameters;
- performing calculations using NJOY;
- calculation of the matrices.

In this work, covariance matrices for total cross-sections from the TENDL-2023 library and earlier versions of TENDL were used.

The parameter uncertainties were chosen according to the results of Refs. [25,26]. The parameters of the arc-dpa model were varied within 20%, and the NRT model within 15%, with E_d values varied by 20% in both cases.

It is important to note that the main contribution to the uncertainty of the displacement cross-sections comes from the model parameters used to calculate the number of defects.

The resulting covariance matrices and displacement cross-sections were recorded in the ENDF-6 format.

3. Displacement cross-sections

3.1 Data from 10^{-5} eV up to maximum available energy in files

Displacement cross-sections were obtained for all stable isotopes from lithium to bismuth, and these were then used for the calculation of cross-sections for natural isotope mixtures.

Data from the libraries were utilized as they were, up to the maximum available energy. Calculations were performed using the arc-dpa and NRT models. No additional adjustments were made to avoid the possible data jumps around 20-30 MeV [12]. An example of the data obtained is shown in Fig.3.

Displacement cross-sections were written in the ENDF-6 format and processed into the ACE format with the NJOY code. Cross-sections are presented on a point-by-point basis, without averaging by energy intervals.

The data obtained can be downloaded from the webpage [46].

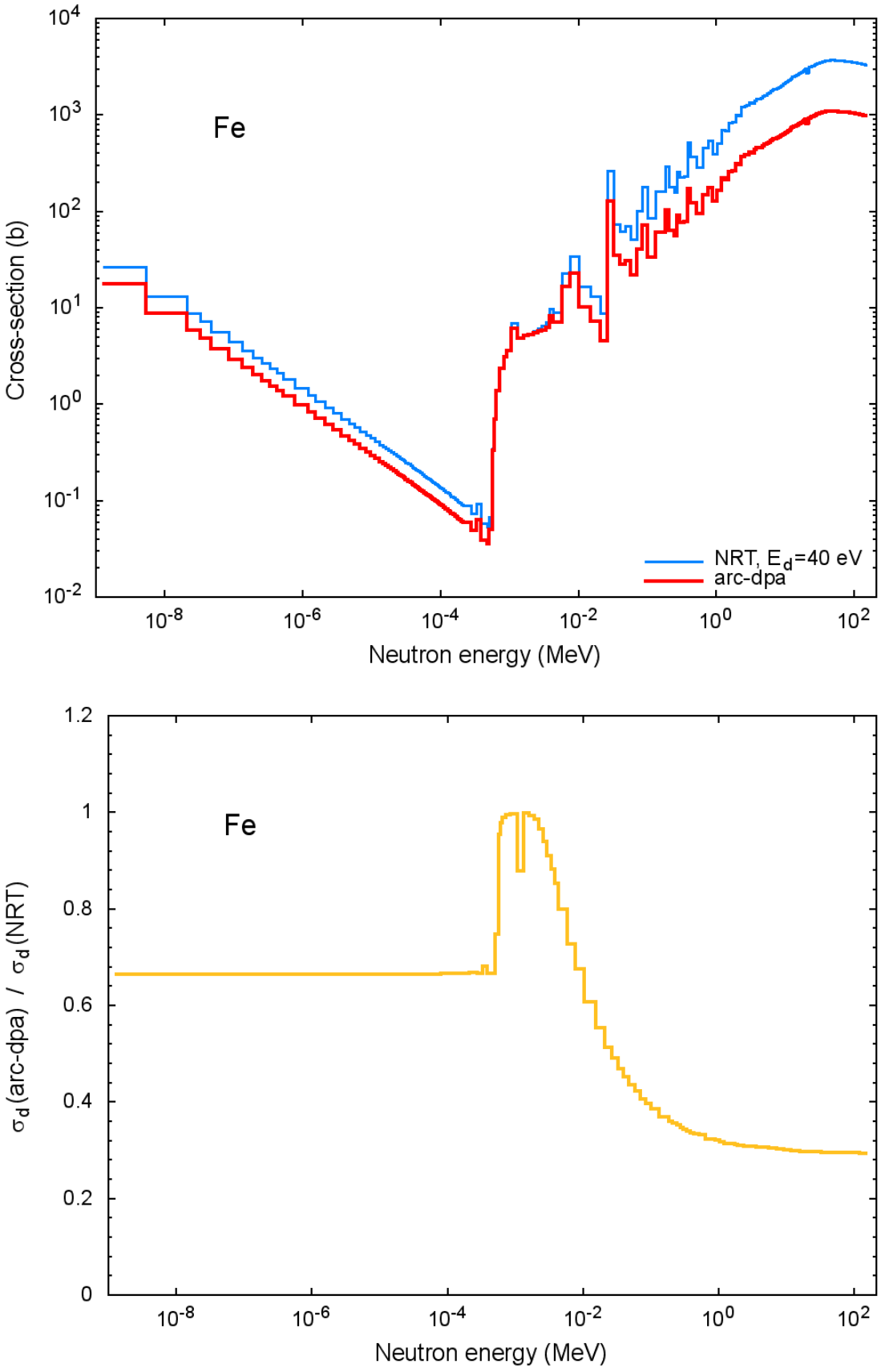

Fig.3 Displacement cross-sections (upper figure) for iron obtained using the arc-dpa model and NRT model and data from JEFF-4 and the ratio of cross-sections (lower figure). For a better graphical representation, the cross-sections were averaged using 304 energy groups.

3.2 Data extended to 200 MeV

A number of library files contain data only up to a maximum energy below 200 MeV. To facilitate and unify the use of displacement cross-sections at high energies, the data obtained in this work were extended to 200 MeV where necessary for all targets from lithium to bismuth. The extension of the displacement cross-sections is discussed above in Section 2.4.

For certain materials, the displacement cross-sections were smoothed to avoid non-physical jumps and to ensure proper data merging. Smoothing was applied only to targets for which the data were extended.

Examples of data extension are shown in Figures 4-11.

The resulting data in ENDF-6 and ACE formats can be downloaded from the webpage [46]. The same page also contains plots for all materials whose cross-sections were extended up to 200 MeV.

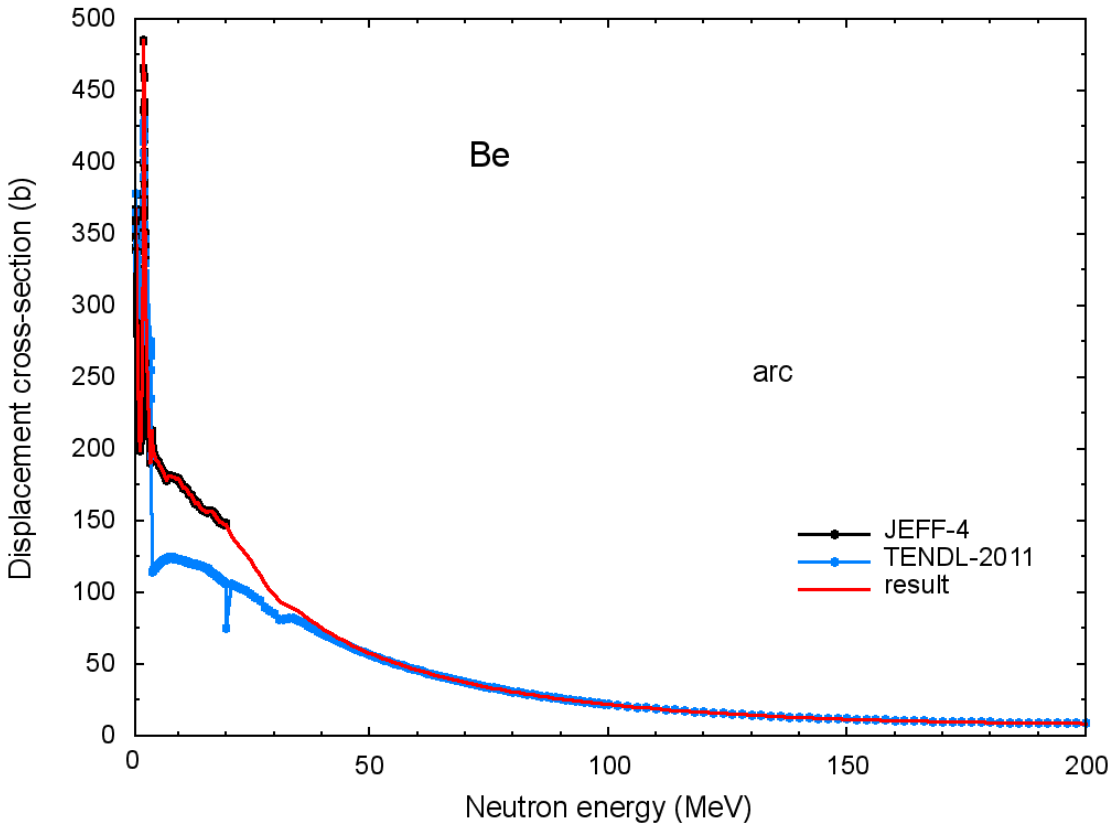

Fig.4 Example of the extension of arc-dpa displacement cross-sections for beryllium calculated using JEFF-4 applying data from TENDL.

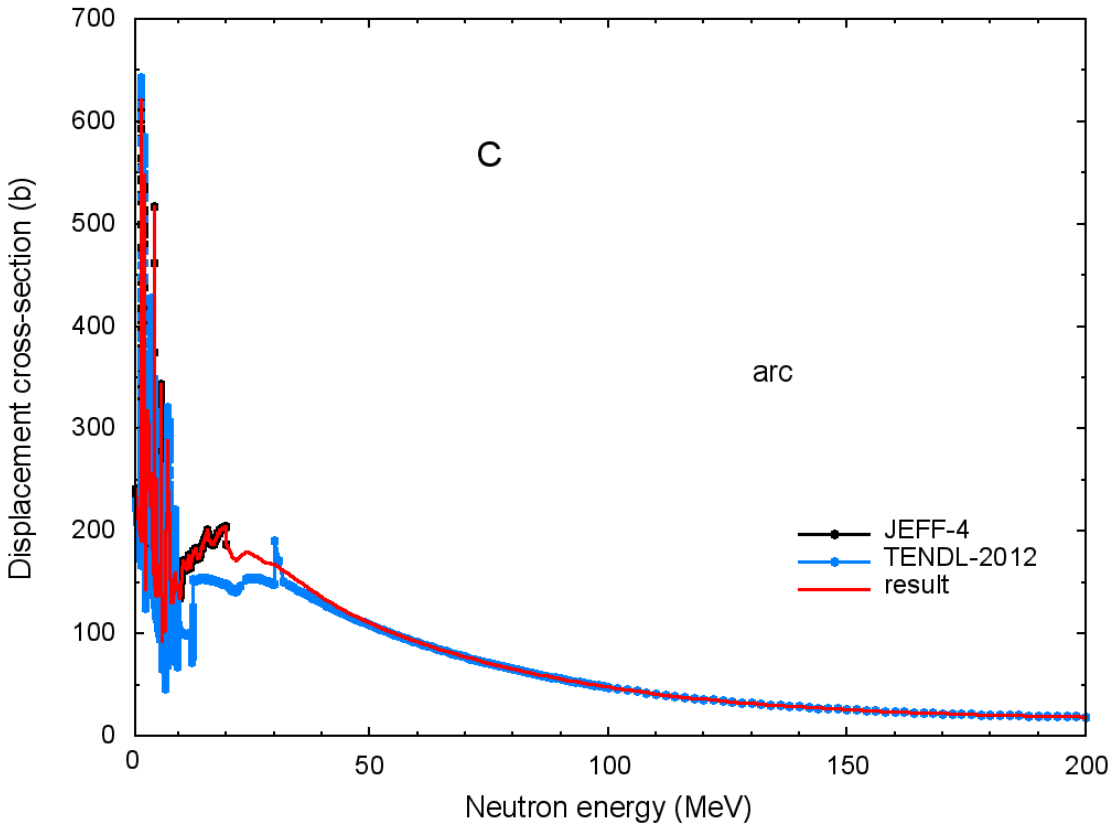

Fig.5 The same as in Fig.4 but for carbon.

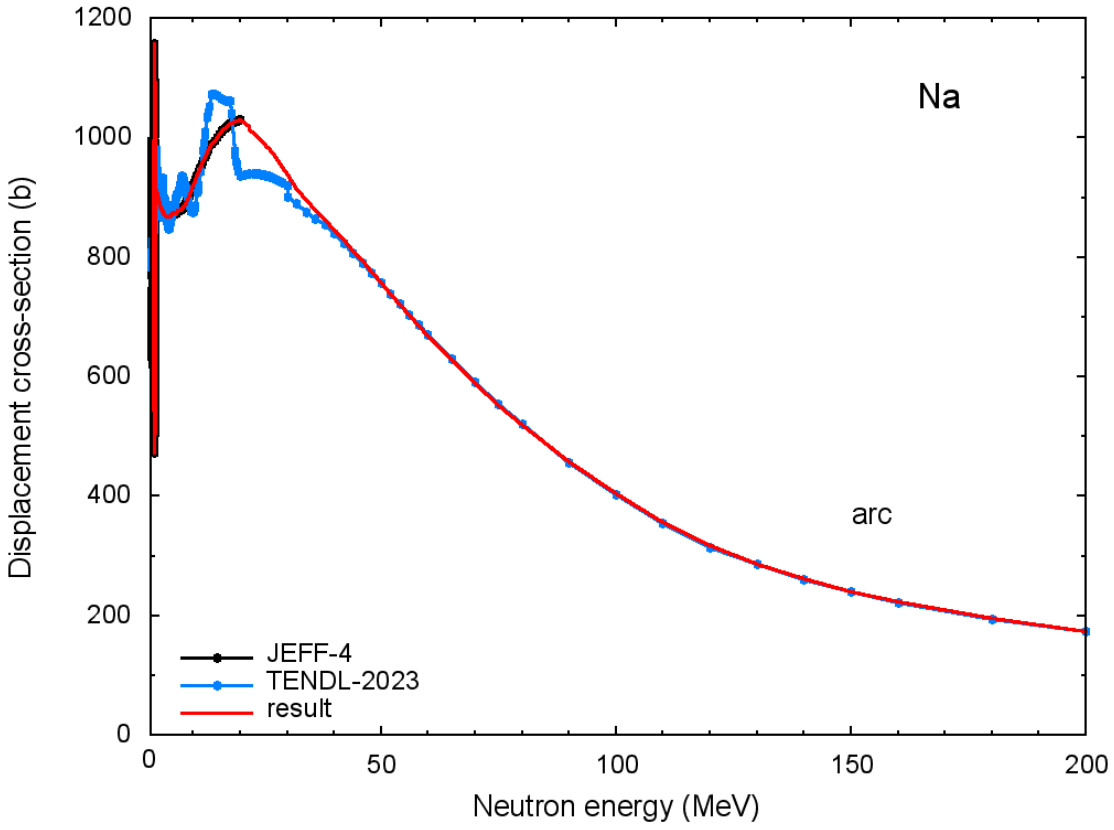

Fig.6 The same as in Fig.4 but for sodium.

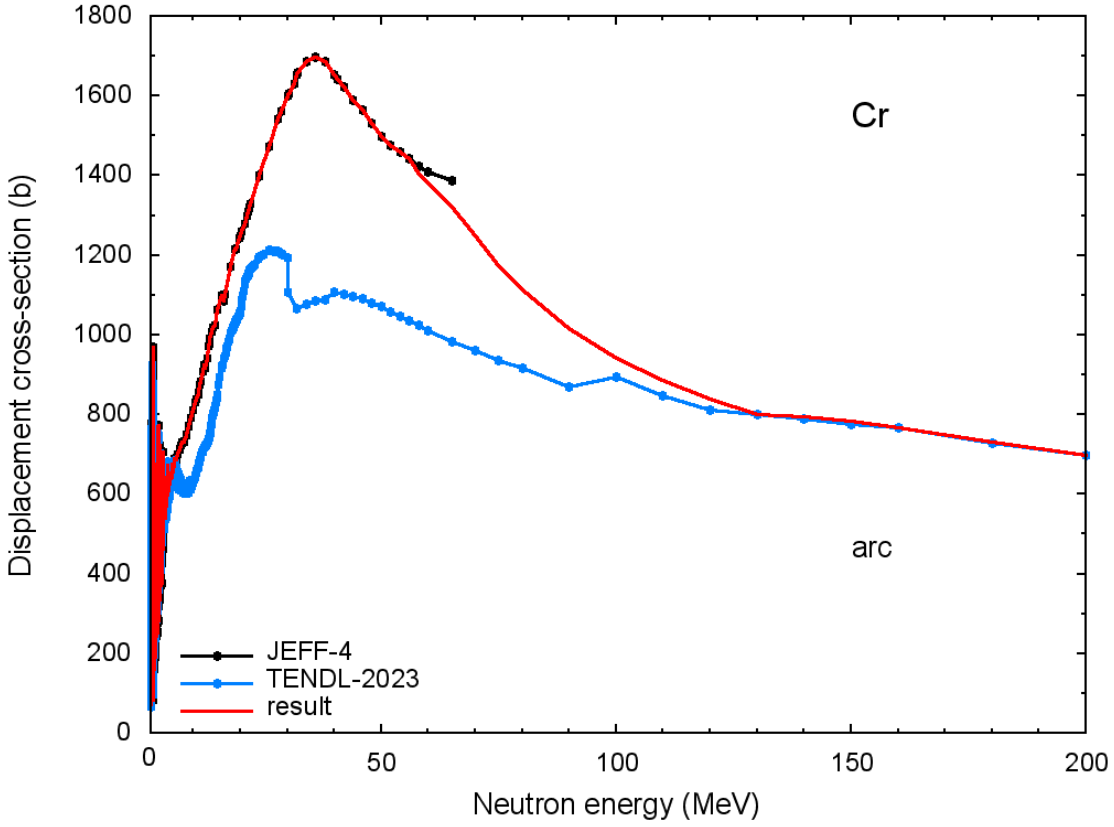

Fig.7 The same as in Fig.4 but for chromium.

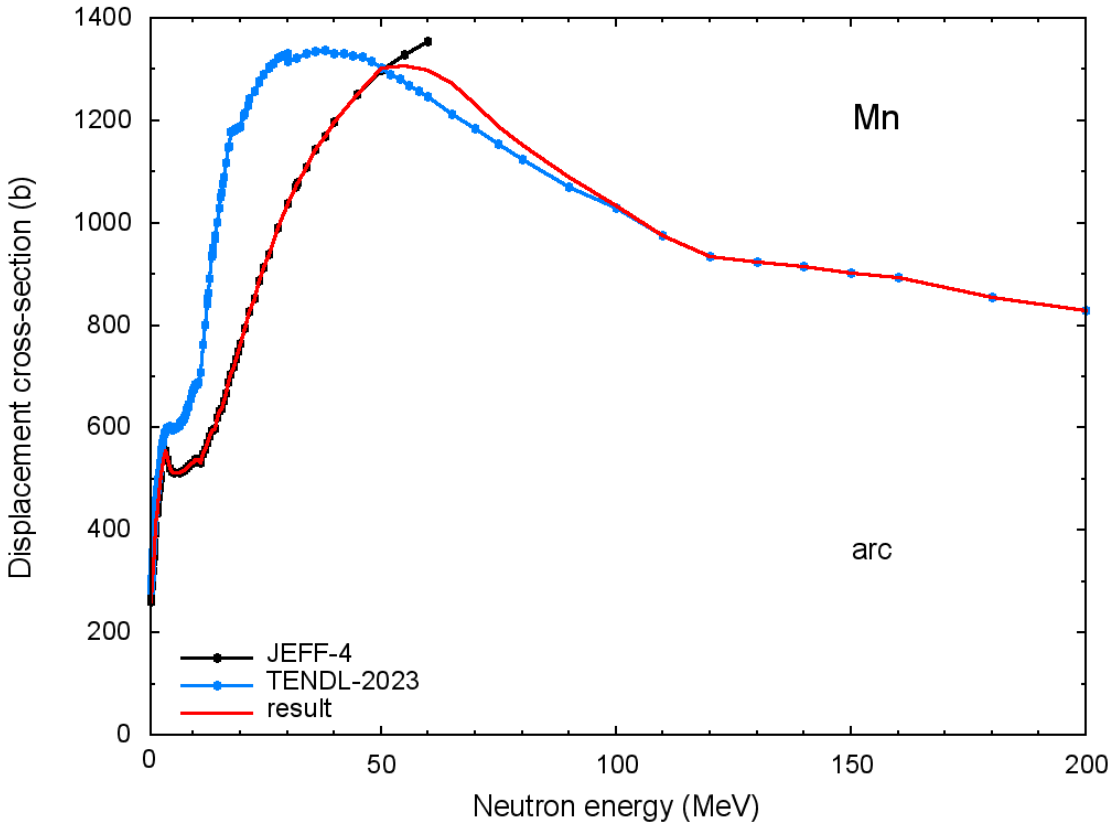

Fig.8 The same as in Fig.4 but for manganese.

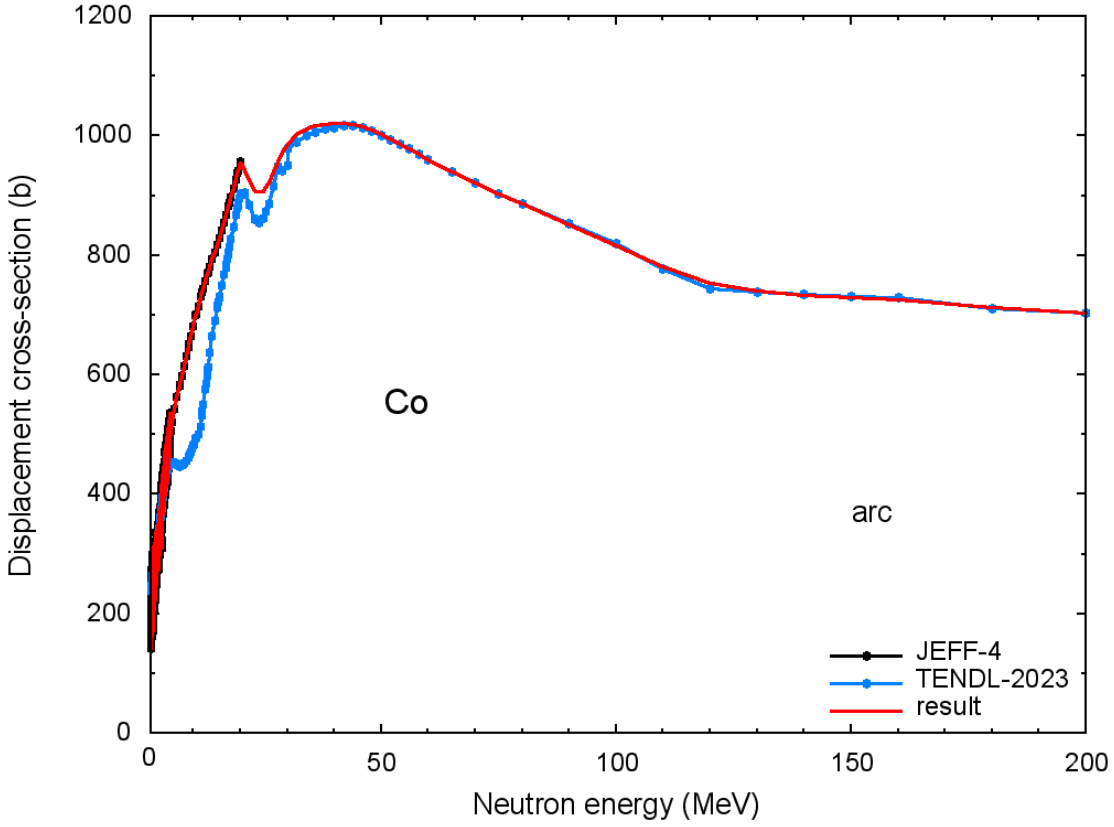

Fig.9 The same as in Fig.4 but for cobalt.

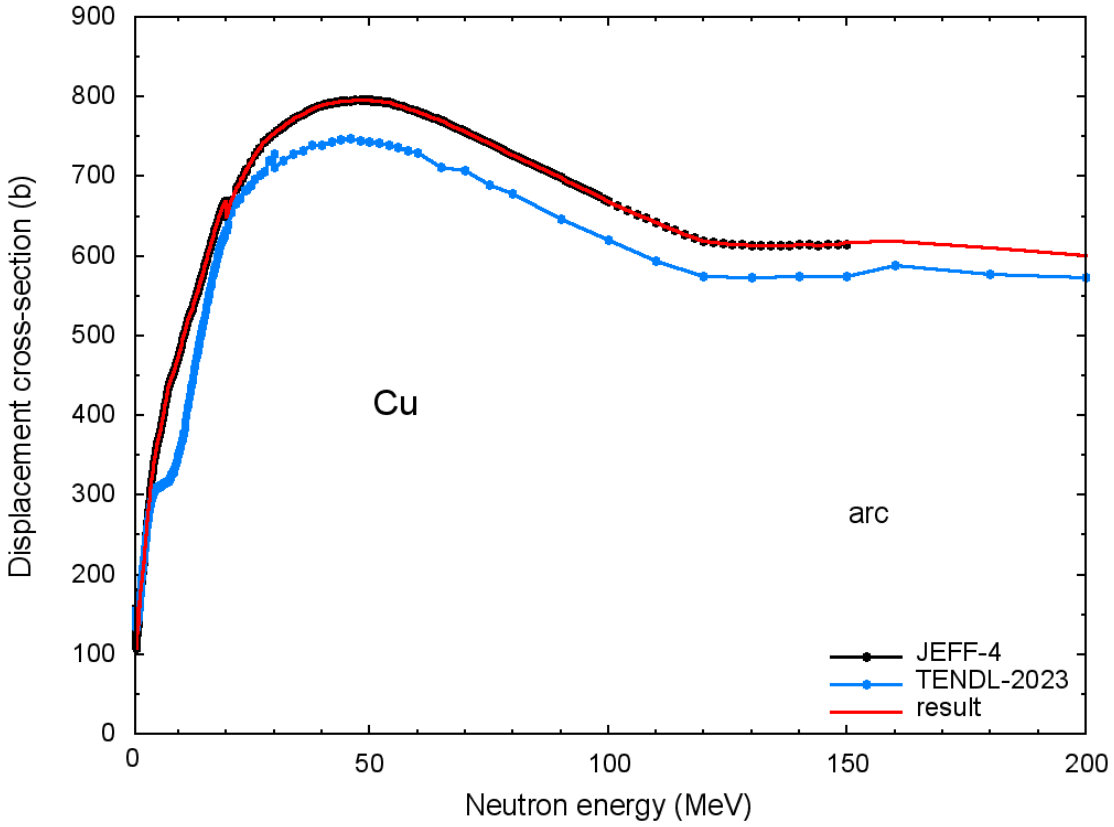

Fig.10 The same as in Fig.4 but for copper.

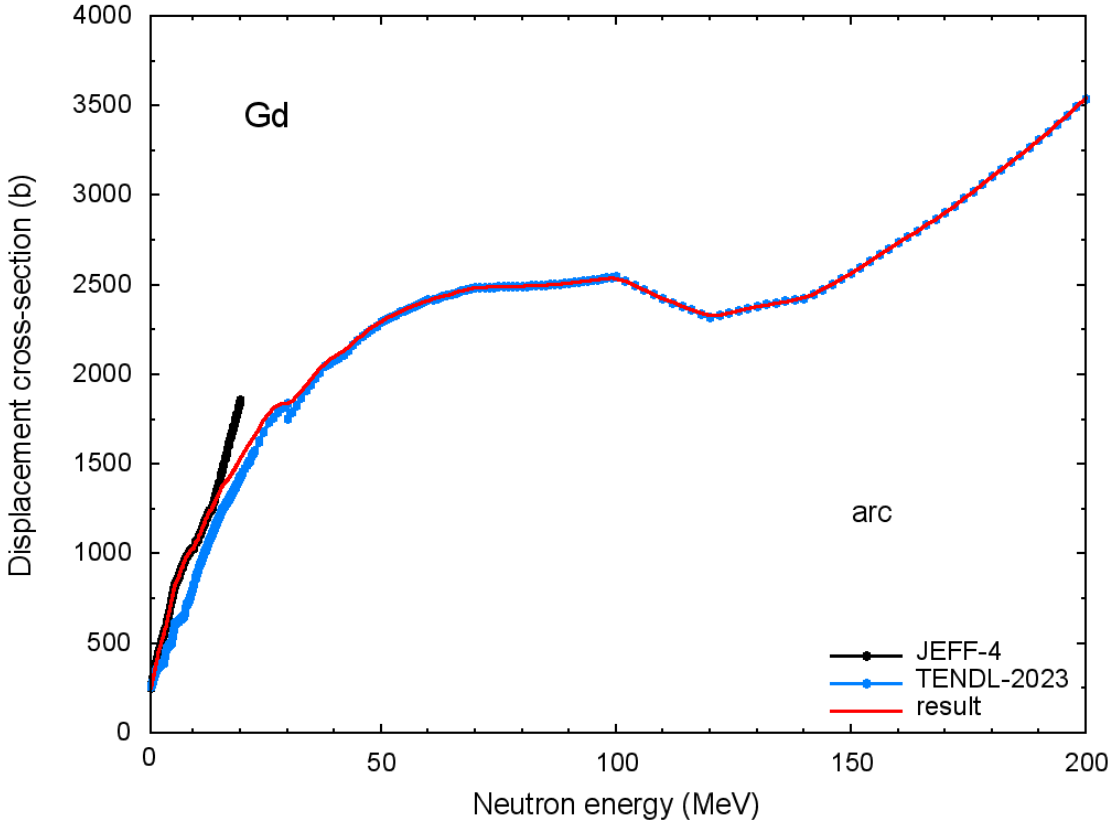

Fig.11 The same as in Fig.4 but for gadolinium.

4. Conclusion

Displacement cross-sections were calculated for materials from lithium to bismuth using the arc-dpa model and the NRT model. For this purpose, nuclear data from JEFF-4.0, ENDF/B-VIII.1, JENDL-5 (July 2024), and TENDL-2023 (August 2024) were used.

The resulting cross-sections for each library were extended using TENDL data up to incident neutron energies of 200 MeV.

The displacement cross-sections obtained from JEFF-4 were provided with covariance matrices.

The data were recorded in ENDF-6 format, processed using the NJOY code, and written in ACE format separately for each library.

The resulting displacement cross-sections are available for download on the webpage [46].

Acknowledgement

This work has been carried out within the framework of the EUROfusion Consortium and has received funding from the Euratom research and training programme 2014-2018 and 2019-2020 under grant agreement No 633053. The views and opinions expressed herein do not necessarily reflect those of the European Commission.

References

[1] A.Yu. Konobeyev, U. Fischer, P.E. Pereslavtsev, S.P. Simakov, Displacement cross-sections, DXS files (2018), https://www-nds.iaea.org/public/download-endf/DXS/

[2] A.Yu. Konobeyev, U. Fischer, S.P.,Simakov, Improved atomic displacement cross-sections for proton irradiation of aluminium, iron, copper, and tungsten at energies up to 10 GeV, *Nucl. Instr. Meth. Phys. Res.* B431 (2018) 55.

[3] A.Yu. Konobeyev, U. Fischer, S.P.,Simakov, Atomic displacement cross-sections for neutron irradiation of materials from Be to Bi calculated using the arc-dpa model, *Nuclear Engineering and Technology*, 51 (2019) 170.

[4] The Joint Evaluated Fission and Fusion File JEFF-3.3 (2017), DPA Sublibrary, https://www.oecd-nea.org/dbdata/jeff/jeff33/index.html#dpa

[5] K. Nordlund, S.J. Zinkle, A.E. Sand, F. Granberg, R.S. Averback, R. Stoller, T. Suzudo, L. Malerba, F. Banhart, W.J. Weber, F. Willaime, S.L. Dudarev, D. Simeone, Improving atomic displacement and replacement calculations with physically realistic damage models, *Nature Communications,* 9 (2018) 1084, https://doi.org/10.1038/s41467-018-03415-5

[6] M.J. Norgett, M.T. Robinson, I.M. Torrens, A proposed method of calculating displacement dose rates, *Nucl. Eng. Des.* 33 (1975) 50.

[7] M.T. Robinson, Basic physics of radiation damage production, *J. Nucl. Mater.* 216 (1994) 1.

[8] D.A. Brown, M.B. Chadwick, R. Capote, A.C. Kahler, A. Trkov, M.W. Herman, A.A. Sonzogni, Y. Danon, A.D. Carlson, M. Dunn, D.L. Smith, G.M. Hale, G. Arbanas, R. Arcilla, C.R. Bates, B. Beck, B. Becker, F. Brown, R.J. Casperson, J. Conlin, D.E. Cullen, M.-A. Descalle, R. Firestone, T. Gaines, K.H. Guber, A.I. Hawari, J. Holmes, T.D. Johnson, T. Kawano, B.C. Kiedrowski, A.J. Koning, S. Kopecky, L. Leal, J.P. Lestone, C. Lubitz, J.I. Márquez Damián, C.M. Mattoon, E.A. McCutchan, S. Mughabghab, P. Navratil, D. Neudecker, G.P.A. Nobre, G. Noguere, M. Paris, M.T. Pigni, A.J. Plompen, B. Pritychenko, V.G. Pronyaev, D. Roubtsov, D. Rochman, P. Romano, P. Schillebeeckx, S. Simakov, M. Sin, I. Sirakov, B. Sleaford, V. Sobes, E.S. Soukhovitskii, I. Stetcu, P. Talou, I. Thompson, S. van der Marck, L. Welser-Sherrill, D. Wiarda, M. White, J.L. Wormald, R.Q. Wright, M. Zerkle, G. Žerovnik, Y. Zhu, ENDF/B-VIII.0: The 8th major release of the nuclear reaction data library with CIELO-project cross sections, new standards and thermal scattering data, *Nuclear Data Sheets*, 148, (2018) 1.

[9] A.J.M. Plompen, O.Cabellos, C.De Saint Jean, M. Fleming, A. Algora, M. Angelone, P. Archier, E. Bauge, O. Bersillon, A. Blokhin, F. Cantargi, A. Chebboubi, C. Diez, H. Duarte, E. Dupont, J. Dyrda, B. Erasmus, L. Fiorito, U. Fischer, D. Flammini, D. Foligno, M. R. Gilbert, J. R. Granada, W. Haeck, F.-J. Hambsch, P. Helgesson, S. Hilaire, I. Hill, M. Hursin, R. Ichou, R. Jacqmin, B. Jansky, C. Jouanne, M. A. Kellett, D. H. Kim, H. I. Kim, I. Kodeli, A. J. Koning, A. Yu. Konobeyev, S. Kopecky, B. Kos, A. Krása, L. C. Leal, N. Leclaire, P. Leconte, Y. O. Lee, H. Leeb, O. Litaize, M. Majerle, J. I Márquez Damián, F. Michel-Sendis, R. W. Mills, B. Morillon, G. Noguère, M. Pecchia, S. Pelloni, P. Pereslavtsev, R. J. Perry, D. Rochman, A. Röhrmoser, P. Romain, P. Romojaro, D. Roubtsov, P. Sauvan, P. Schillebeeckx, K. H. Schmidt, O. Serot, S. Simakov, I. Sirakov, H. Sjöstrand, A. Stankovskiy, J. C. Sublet, P. Tamagno, A. Trkov, S. van der Marck, F. Álvarez-Velarde, R. Villari, T. C. Ware, K. Yokoyama, G. Žerovnik, The joint evaluated fission and fusion nuclear data library, JEFF-3.3, *Eur. Phys. J. A*, 56 (2020) 181.

[10] K. Shibata, O. Iwamoto, T. Nakagawa, N. Iwamoto, A. Ichihara, S. Kunieda, S. Chiba, K. Furutaka, N. Otuka, T. Ohsawa, T. Murata, H. Matsunobu, A. Zukeran, S. Kamada, J. Katakura: JENDL-4.0: A new library for nuclear science and engineering, *J. Nucl. Sci. Technol.*, 48(1) (2011) 1.

[11] A.J. Koning and D. Rochman, Modern nuclear data evaluation with the TALYS code system, *Nuclear Data Sheets* 113 (2012) 2841; TENDL-2017 (December 30, 2017), https://tendl.web.psi.ch/tendl_2017/tendl2017.html

[12] A.Yu. Konobeyev, D. Leichtle, Arc-dpa and NRT displacement cross-sections for neutron irradiation of materials from Be to Bi calculated using JEFF-4T1, ENDF/B-VIII, JENDL-5, and TENDL-2021 data, KIT Scientific Working Papers 190 (2022); https://dx.doi.org/10.5445/IR/1000147764

[13] Joint Evaluated Fission and Fusion (JEFF) Nuclear Data Library, JEFF-4T1 (Test library) (February 2022), https://www.oecd-nea.org/dbdata/jeff/jeff40/t1/

[14] O. Iwamoto, N. Iwamoto, S. Kunieda, F. Minato, S. Nakayama, Y. Abe, K. Tsubakihara, S. Okumura, C. Ishizuka, T. Yoshida, S. Chiba, N. Otuka, J.-Ch. Sublet, H. Iwamoto, K. Yamamoto, Y. Nagaya, K. Tada, C. Konno, N. Matsuda, K. Yokoyama, H. Taninaka, A. Oizumi, M. Fukushima, S. Okita, G. Chiba, S. Sato, M. Ohta, S. Kwon, Japanese evaluated nuclear data library version 5: JENDL-5, *J. Nucl. Sci. Technol.,* 60 (2023) 1, https://doi.org/10.1080/00223131.2022.2141903

[15] A.J. Koning, D. Rochman, J. Sublet, N. Dzysiuk, M. Fleming, S. van der Marck, TENDL: complete nuclear data library for innovative nuclear science and technology, *Nuclear Data Sheets* 155 (2019) 1; TENDL-2021 (December 30, 2021), https://tendl.web.psi.ch/tendl_2021/tendl2021.html

[16] Joint Evaluated Fission and Fusion (JEFF) Library version 4.0. NEA Data Bank GitLab platform, https://databank.io.oecd-nea.org/data/jeff/40/

[17] G. Nobre, D.A. Brown, R. Arcilla, R. Coles, B. Shu, Progress towards the ENDF/B-VIII.1 release, *EPJ Web of Conferences* 294 (2024) 04004. https://dx.doi.org/10.1051/epjconf/202429404004; ENDF B-VIII.1 Full Library: https://www.nndc.bnl.gov/endf-releases/?version=B-VIII.1

[18] JENDL-5 https://wwwndc.jaea.go.jp/jendl/j5/j5.html and https://wwwndc.jaea.go.jp/jendl/j5/JENDL-5_Errata.html; see also Ref.[14]

[19] TENDL-2023 Nuclear data library, Neutron sub-library, Updated in August 2024, https://tendl.web.psi.ch/tendl_2023/neutron_html2024/neutron.html, see also Ref.[15].

[20] K. Nordlund, private communication (2016).

[21] A.Yu. Konobeyev, U. Fischer, Yu.A. Korovin, S.P. Simakov, Evaluation of effective threshold displacement energies and other data required for the calculation of advanced atomic displacement cross-sections, *Nuclear Energy and Technology*, 3 (2017) 169.

[22] A.Yu. Konobeyev, U. Fischer, S.P. Simakov, Status of the evaluation of n+^{9}Be displacement cross-section using advance defect production model, NEA Nuclear Data Week, 25-29 November 2019, EFFDOC-1411 (2019), https://www.oecd-nea.org/dbdata/nds_effdoc/effdoc-1411.pdf; https://dx.doi.org/10.13140/RG.2.2.26516.24965

[23] R.E. MacFarlane, D.W. Muir, R.M. Boicourt, A.C. Kahler, J.L. Conlin, W. Haeck, The NJOY nuclear data processing system, version 2016; Report LANL LA-UR-17-20093 (2019); The NJOY Nuclear Data Processing System, version 2016, NJOY2016.78 (February 2025), https://github.com/njoy/NJOY2016

[24] D.E. Cullen, PREPRO 2023 - ENDF/B Pre-processing Codes, IAEA-NDS-0241, https://dx.doi.org/10.61092/iaea.ts9j-05x7; https://www-nds.iaea.org/public/endf/prepro/

[25] A.Yu. Konobeyev, U. Fischer, S.P. Simakov, Uncertainties of displacement cross-sections for iron and tungsten at neutron irradiation energies above 0.1 MeV, KIT Scientific Working Papers 49 (2016), https://publikationen.bibliothek.kit.edu/1000057548

[26] A.Yu. Konobeyev, U. Fischer, S.P. Simakov, Uncertainty assessment for the number of defects calculated using the NRT damage model, KIT Scientific Working Papers 70 (2017), https://dx.doi.org/10.5445/IR/1000074095

[27] A.Yu. Konobeyev, U. Fischer, S.P. Simakov, Neutron displacement cross-sections for materials from Be to U calculated using the arc-dpa concept, Proc. 13th International Topical Meeting on the Applications of Accelerators (AccApp'17), July 31-August 4, 2017, Quebec, http://accapp17.org/wp-content/2017/data/pdfs/110-22892.pdf

[28] A.Yu. Konobeyev, U. Fischer, Yu.A. Korovin, S.P. Simakov, IOTA-2017: a code for the simulation of ion transport in materials, KIT Scientific Working Papers 63 (2017), https://publikationen.bibliothek.kit.edu/1000077011

[29] W. Yin, A.Yu. Konobeyev, D. Leichtle, L. Cao, Calculation of displacement damage cross-section for charged particles at energies up to 100 GeV, *J. Nucl. Mater.* 573 (2023) 154143.

[30] C.H.M. Broeders, A.Yu. Konobeyev, Defect production efficiency in metals under neutron irradiation, *J. Nucl. Mater.* 328 (2004) 197.

[31] W. Yin, A.Yu. Konobeyev, D. Leichtle, L. Cao, General displacement function for displacement damage cross-section calculation, *Nucl. Instr. Meth. Phys. Res.* B538 (2023) 157.

[32] A. Dunlop, D. Lesueur, P. Legrand, H. Dammak, Effects induced by high electronic excitations in pure metals:a detailed study in iron, *Nucl. Instr. Meth. Phys. Res.* B90 (1994) 330.

[33] W. Yin, private communication (2022).

[34] A.E. Sand, K. Nordlund, On the lower energy limit of electronic stopping in simulated collision cascades in Ni, Pd and Pt, *J. Nucl. Mater.* 456 (2015) 99.

[35] G.A. Greene, C.L. Snead Jr., C.C. Finfrock, A.L. Hanson, M.R. James, W.F. Sommer, E.J. Pitcher, L.S. Waters, Direct measurements of displacement cross sections in copper and tungsten under irradiation by 1.10-GeV and 1.94-GeV protons at 4.7 K, Topical Meeting of the American Nuclear Society. Accelerator Applications in a Nuclear Renaissance (AccApp '03), 1-5 Jun 2003. San Diego.

[36] Y. Iwamoto, T. Yoshiie, M. Yoshida, T. Nakamoto, M. Sakamoto, Y. Kuriyama, T. Uesugi, Y. Ishi, Q. Xu, H. Yashima, F. Takahashi, Y. Mori, T. Ogitsu, Measurement of the displacement cross-section of copper irradiated with 125 MeV protons at 12 K, *J. Nucl. Mater,* 458 (2015) 369.

[37] Y. Iwamoto, M. Yoshida, T. Yoshiie, D. Satoh, H. Yashima, H. Matsuda, S. Meigo, T. Shima, Measurement of displacement cross sections of aluminum and copper at 5 K by using 200 MeV protons, *J. Nucl. Mater.* 508 (2018) 195.

[38] H. Matsuda, S. Meigo, Y. Iwamoto, M. Yoshida, S. Hasegawa, F. Maekawa, H. Iwamoto, T. Nakamoto, T. Ishida, S. Makimura, Measurement of displacement cross-sections of copper and iron for proton with kinetic energies in the range 0.4 – 3 GeV, *J. Nucl. Sci. Technol.* 57 (2020) 1141; https://doi.org/10.1080/00223131.2020.1771453

[39] Y. Iwamoto, M. Yoshida, H. Matsuda, S. Meigo, D. Satoh, H. Yashima, A. Yabuuchi, T. Shima, Measurements of displacement cross section of tungsten under 389-MeV proton irradiation and thermal damage recovery, *Materials Science Forum*, 1024 (2020) 95; https://doi.org/10.4028/www.scientific.net/MSF.1024.95

[40] S.P. Simakov, U. Fischer, A.J. Koning, A.Yu. Konobeyev, D.A. Rochman, Iron NRT- and arc-displacement cross sections and their covariances, *Nuclear Materials and Energy*, 15 (2018) 244; https://doi.org/10.1016/j.nme.2018.05.006

[41] Standard practice for characterizing neutron exposures in iron and low alloy steels in terms of displacements per atom (dpa), ASTM E693-12, June 1, 2012.

[42] HEATR module with additions, send an email to alexander.konobeev@kit.edu

[43] A.Yu. Konobeyev, C.H.M. Broeders, U. Fischer Calculation of displacement cross sections at intermediate and high energies of primary particles using results of molecular dynamics simulations, Proc. Int. Conf. Nucl. Data for Sci. and Technol., Nice, April 22-27 2007, https://doi.org/10.1051/ndata:07754

[44] J. Raynal, ECIS96, Proc. Specialists' Meeting on the Nucleon Nucleus Optical Model up to 200 MeV, Bruyères-le-Chatel, France, Nov. 13-15, 1996, http://www.nea.fr/html/science/om200/raynal.pdf

[45] A.J. Koning, J.P. Delaroche, Local and global nucleon optical models from 1 keV to 200 MeV, *Nucl. Phys.* A713 (2003) 231.

[46] A.Yu. Konobeyev, D. Leichtle, Evaluated atomic displacement cross-sections using arc-dpa and NRT model (August 2025), https://bwsyncandshare.kit.edu/s/83HW426X4XQEQwZ

Appendix

Defect generation efficiency calculated for beryllium, aluminium, iron, copper, and tungsten using various neutron spectra

The arc-dpa model and the results of arc-dpa-BCA simulations were used to calculate the defect generation efficiency for various irradiation conditions (neutron spectra). For the arc-dpa-BCA calculations, the same parameters and values as in Ref.[12] were used.

Nuclear data were taken from the JEFF-4.0 library. Since extended data up to 200 MeV were not used here, in some cases the values of efficiency (η) for beryllium were found to be zero.

The neutron spectra used are partially discussed in Ref.[30].

Part 1 presents the absolute values of the defect generation efficiency η. The values presented here can be compared with the experimental data in Tables 2 and 4 of Ref.[30].

Part 2 illustrates the relative difference (D) in efficiencies calculated using arc-dpa-BCA and "pure" arc-dpa calculations. The value D highlights the uncertainty in defect generation efficiency calculations that could be expected if arc-dpa-BCA simulations are not employed.

The following values of average threshold energy E_d were used in calculations: 31.2 eV for Be, 27 eV for Al, 40 eV for Fe, 33 eV for Cu, and 70 eV for W.

Designations:

`arc-dpa` : the calculation of the number of generated defects was performed using arc-dpa model without BCA simulations

`arc-dpa--BCA` : the number of defects was obtained in arc-dpa - BCA simulations

`Z` : atomic number of material

`Carc and Barc` : arc-dpa parameters

`spectrum` : type of the neutron spectrum $\varphi(E)$ [30]

`standard NRT (barn)` : the radiation damage rate $\int \sigma_{NRT}(E)\varphi(E)dE$, where $\sigma_{NRT}(E)$ is the displacement cross-section calculated using the NRT model

modified (barn) : the radiation damage rate $\int \sigma_D(E)\varphi(E)dE$, where $\sigma_D(E)$ is the displacement cross-section calculated using the arc-dpa model or results of arc-dpa-BCA simulations depending on the heading preceding each table

efficiency : the efficiency η of the defect generation: $\int \sigma_D(E)\varphi(E)dE / \int \sigma_{NRT}(E)\varphi(E)dE$

Part I

Be, arc-dpa:

4	0.6678 -0.8200 * Z	Carc	Barc	
Z	spectrum	standard NRT barn	modified barn	efficiency
4	APWR	318.4	215.2	0.676
4	KWO/PWR	243.0	164.1	0.676
4	TRIGA/TRADE	111.2	75.1	0.675
4	SNR-2	356.5	241.3	0.677
4	TTB (FRM)	158.3	107.0	0.676
4	Fission TETA=1.35 MeV	437.9	294.8	0.673
4	Fusion spectrum	269.1	182.1	0.677
4	14.8 MeV neutrons	235.3	158.6	0.674
4	(d,Be)n for 40 MeV deuterons		zero values	
4	HFIR	141.1	95.4	0.676
4	PWR Robinson2	253.5	171.3	0.676
4	LWR (PWR oder BWR)	349.0	235.6	0.675
4	EPRI BWR 1/4T	307.7	207.6	0.675
4	EPRI BWR 3/4T	342.4	231.2	0.675
4	EPRI Pwr 1/4T	334.4	225.8	0.675
4	EPRI Pwr 3/4T	345.3	233.3	0.676
4	LWR Kori Unit 3	284.6	192.3	0.676
4	OWR Omega West Reactor	166.2	112.3	0.675
4	EBR-II exp breeder reactor	464.8	313.4	0.674
4	Bor-60 Sevastianov	478.3	322.4	0.674
4	RTNS-II Fusion simulation sp	233.5	157.4	0.674
4	ITER FW	282.3	190.7	0.676
4	DEMO	269.1	182.1	0.677
4	IFMIF		zero values	

Be, arc-dpa—BCA:

Z	spectrum	standard NRT barn	modified barn	efficiency
4	APWR	318.4	223.7	0.703
4	KWO/PWR	243.0	171.0	0.704
4	TRIGA/TRADE	111.2	78.4	0.705
4	SNR-2	356.5	249.2	0.699
4	TTB (FRM)	158.3	111.5	0.704
4	Fission TETA=1.35 MeV	437.9	309.3	0.706
4	Fusion spectrum	269.1	189.2	0.703
4	14.8 MeV neutrons	235.3	167.7	0.713
4	(d,Be)n for 40 MeV deuterons	zero values		----------
4	HFIR	141.1	99.3	0.704
4	PWR Robinson2	253.5	178.0	0.702
4	LWR (PWR oder BWR)	349.0	244.8	0.701
4	EPRI BWR 1/4T	307.7	216.2	0.703
4	EPRI BWR 3/4T	342.4	240.1	0.701
4	EPRI Pwr 1/4T	334.4	234.7	0.702
4	EPRI Pwr 3/4T	345.3	241.7	0.700
4	LWR Kori Unit 3	284.6	199.5	0.701
4	OWR Omega West Reactor	166.2	117.1	0.704
4	EBR-II exp breeder reactor	464.8	325.9	0.701
4	Bor-60 Sevastianov	478.3	335.0	0.700
4	RTNS-II Fusion simulation sp	233.5	166.4	0.713
4	ITER FW	282.3	198.7	0.704
4	DEMO	269.1	189.2	0.703
4	IFMIF	zero values		----------

Al, arc-dpa:

13 0.4426 -0.8200 * Z Carc Barc

Z	spectrum	standard NRT barn	modified barn	efficiency
13	APWR	711.4	318.9	0.448
13	KWO/PWR	613.0	274.4	0.448
13	TRIGA/TRADE	317.0	141.9	0.448

13	SNR-2	574.3	259.1	0.451
13	TTB (FRM)	405.9	181.8	0.448
13	Fission TETA=1.35 MeV	1481.5	660.8	0.446
13	Fusion spectrum	797.5	356.6	0.447
13	14.8 MeV neutrons	2305.1	1024.1	0.444
13	(d,Be)n for 40 MeV deuterons	1989.0	884.6	0.445
13	HFIR	356.8	159.9	0.448
13	PWR Robinson2	539.6	242.0	0.448
13	LWR (PWR oder BWR)	723.6	324.4	0.448
13	EPRI BWR 1/4T	738.3	330.4	0.448
13	EPRI BWR 3/4T	665.8	298.7	0.449
13	EPRI Pwr 1/4T	717.0	321.2	0.448
13	EPRI Pwr 3/4T	567.5	255.2	0.450
13	LWR Kori Unit 3	528.7	237.5	0.449
13	OWR Omega West Reactor	461.9	206.7	0.447
13	EBR-II exp breeder reactor	996.7	446.9	0.448
13	Bor-60 Sevastianov	955.0	428.6	0.449
13	RTNS-II Fusion simulation sp	2246.1	998.0	0.444
13	ITER FW	994.3	443.9	0.446
13	DEMO	797.4	356.5	0.447
13	IFMIF	1590.7	708.8	0.446

Al, arc-dpa—BCA:

Z	spectrum	standard NRT barn	modified barn	efficiency
13	APWR	711.4	321.1	0.451
13	KWO/PWR	613.0	276.8	0.451
13	TRIGA/TRADE	317.0	143.4	0.452
13	SNR-2	574.3	260.0	0.453
13	TTB (FRM)	405.9	183.3	0.452
13	Fission TETA=1.35 MeV	1481.5	668.4	0.451
13	Fusion spectrum	797.5	364.8	0.457
13	14.8 MeV neutrons	2305.1	1071.5	0.465
13	(d,Be)n for 40 MeV deuterons	1989.0	918.3	0.462
13	HFIR	356.8	161.3	0.452
13	PWR Robinson2	539.6	243.4	0.451
13	LWR (PWR oder BWR)	723.6	326.3	0.451

13	EPRI BWR 1/4T	738.3	333.4	0.452
13	EPRI BWR 3/4T	665.8	300.3	0.451
13	EPRI Pwr 1/4T	717.0	323.4	0.451
13	EPRI Pwr 3/4T	567.5	255.9	0.451
13	LWR Kori Unit 3	528.7	238.4	0.451
13	OWR Omega West Reactor	461.9	208.8	0.452
13	EBR-II exp breeder reactor	996.7	449.1	0.451
13	Bor-60 Sevastianov	955.0	430.4	0.451
13	RTNS-II Fusion simulation sp	2246.1	1043.8	0.465
13	ITER FW	994.3	455.5	0.458
13	DEMO	797.4	364.7	0.457
13	IFMIF	1590.7	726.2	0.457

Fe, arc-dpa:

26 0.2860 -0.5680 * Z Carc Barc

Z	spectrum	standard NRT barn	modified barn	efficiency
26	APWR	349.6	113.5	0.325
26	KWO/PWR	324.2	104.1	0.321
26	TRIGA/TRADE	182.7	59.5	0.326
26	SNR-2	233.9	80.0	0.342
26	TTB (FRM)	215.2	69.9	0.325
26	Fission TETA=1.35 MeV	862.8	269.1	0.312
26	Fusion spectrum	593.2	183.7	0.310
26	14.8 MeV neutrons	2626.9	783.9	0.298
26	(d,Be)n for 40 MeV deuterons	2129.7	638.7	0.300
26	HFIR	191.8	62.6	0.326
26	PWR Robinson2	252.9	82.6	0.326
26	LWR (PWR oder BWR)	332.0	107.6	0.324
26	EPRI BWR 1/4T	382.1	121.9	0.319
26	EPRI BWR 3/4T	294.2	96.0	0.326
26	EPRI Pwr 1/4T	339.5	109.5	0.323
26	EPRI Pwr 3/4T	217.9	73.1	0.336
26	LWR Kori Unit 3	220.9	73.6	0.333
26	OWR Omega West Reactor	259.7	83.4	0.321
26	EBR-II exp breeder reactor	449.4	145.9	0.325

26	Bor-60 Sevastianov	412.5	134.8	0.327
26	RTNS-II Fusion simulation sp	2561.4	764.4	0.298
26	ITER FW	798.8	245.2	0.307
26	DEMO	593.2	183.7	0.310
26	IFMIF	1286.4	392.3	0.305

Fe, arc-dpa—BCA:

Z	spectrum	standard NRT barn	modified barn	efficiency
26	APWR	349.6	120.2	0.344
26	KWO/PWR	324.2	111.6	0.344
26	TRIGA/TRADE	182.7	64.3	0.352
26	SNR-2	233.9	82.6	0.353
26	TTB (FRM)	215.2	74.6	0.347
26	Fission TETA=1.35 MeV	862.8	293.4	0.340
26	Fusion spectrum	593.2	223.0	0.376
26	14.8 MeV neutrons	2626.9	1037.6	0.395
26	(d,Be)n for 40 MeV deuterons	2129.7	834.6	0.392
26	HFIR	191.8	66.9	0.349
26	PWR Robinson2	252.9	86.8	0.343
26	LWR (PWR oder BWR)	332.0	113.5	0.342
26	EPRI BWR 1/4T	382.1	131.6	0.344
26	EPRI BWR 3/4T	294.2	100.9	0.343
26	EPRI Pwr 1/4T	339.5	116.3	0.342
26	EPRI Pwr 3/4T	217.9	75.0	0.344
26	LWR Kori Unit 3	220.9	75.9	0.344
26	OWR Omega West Reactor	259.7	90.3	0.348
26	EBR-II exp breeder reactor	449.4	152.5	0.339
26	Bor-60 Sevastianov	412.5	140.5	0.340
26	RTNS-II Fusion simulation sp	2561.4	1012.1	0.395
26	ITER FW	798.8	301.8	0.378
26	DEMO	593.2	223.0	0.376
26	IFMIF	1286.4	477.9	0.371

Cu, arc-dpa:

29 0.1600 -0.6800 * Z Carc Barc

Z	spectrum	standard NRT barn	modified barn	efficiency
29	APWR	430.7	81.5	0.189
29	KWO/PWR	388.9	72.0	0.185
29	TRIGA/TRADE	213.3	39.3	0.184
29	SNR-2	316.2	65.3	0.207
29	TTB (FRM)	254.3	47.4	0.186
29	Fission TETA=1.35 MeV	1009.2	177.5	0.176
29	Fusion spectrum	774.4	137.1	0.177
29	14.8 MeV neutrons	3451.9	573.2	0.166
29	(d,Be)n for 40 MeV deuterons	2814.7	470.0	0.167
29	HFIR	227.6	42.6	0.187
29	PWR Robinson2	321.0	61.2	0.191
29	LWR (PWR oder BWR)	434.4	82.1	0.189
29	EPRI BWR 1/4T	485.8	89.3	0.184
29	EPRI BWR 3/4T	396.5	75.9	0.191
29	EPRI Pwr 1/4T	441.4	82.8	0.188
29	EPRI Pwr 3/4T	314.3	62.9	0.200
29	LWR Kori Unit 3	292.7	57.4	0.196
29	OWR Omega West Reactor	307.9	56.4	0.183
29	EBR-II exp breeder reactor	564.8	105.8	0.187
29	Bor-60 Sevastianov	533.5	100.8	0.189
29	RTNS-II Fusion simulation sp	3371.0	559.8	0.166
29	ITER FW	1026.5	178.1	0.173
29	DEMO	774.9	137.2	0.177
29	IFMIF	1637.3	279.5	0.171

Cu, arc-dpa—BCA:

Z	spectrum	standard NRT barn	modified barn	efficiency
29	APWR	430.7	86.5	0.201
29	KWO/PWR	388.9	77.7	0.200
29	TRIGA/TRADE	213.3	43.0	0.202

29	SNR-2	316.2	67.1	0.212
29	TTB (FRM)	254.3	50.9	0.200
29	Fission TETA=1.35 MeV	1009.2	196.4	0.195
29	Fusion spectrum	774.4	180.1	0.233
29	14.8 MeV neutrons	3451.9	862.7	0.250
29	(d,Be)n for 40 MeV deuterons	2814.7	702.2	0.249
29	HFIR	227.6	46.0	0.202
29	PWR Robinson2	321.0	64.5	0.201
29	LWR (PWR oder BWR)	434.4	86.9	0.200
29	EPRI BWR 1/4T	485.8	97.7	0.201
29	EPRI BWR 3/4T	396.5	80.0	0.202
29	EPRI Pwr 1/4T	441.4	88.4	0.200
29	EPRI Pwr 3/4T	314.3	64.3	0.205
29	LWR Kori Unit 3	292.7	59.1	0.202
29	OWR Omega West Reactor	307.9	61.9	0.201
29	EBR-II exp breeder reactor	564.8	110.7	0.196
29	Bor-60 Sevastianov	533.5	105.0	0.197
29	RTNS-II Fusion simulation sp	3371.0	843.5	0.250
29	ITER FW	1026.5	239.5	0.233
29	DEMO	774.9	180.2	0.233
29	IFMIF	1637.3	374.6	0.229

W, arc-dpa:

74	0.1190 -0.5640	* Z	Carc	Barc	
* Z	spectrum		standard NRT	modified	efficiency
*			barn	barn	
74	APWR		106.5	27.6	0.260
74	KWO/PWR		94.6	23.6	0.250
74	TRIGA/TRADE		50.8	12.7	0.249
74	SNR-2		78.8	24.7	0.314
74	TTB (FRM)		63.6	16.3	0.257
74	Fission TETA=1.35 MeV		238.2	51.9	0.218
74	Fusion spectrum		150.2	32.9	0.219
74	14.8 MeV neutrons		574.6	96.4	0.168
74	(d,Be)n for 40 MeV deuterons		617.9	101.4	0.164
74	HFIR		56.1	14.6	0.261

74	PWR Robinson2	81.5	22.0	0.270
74	LWR (PWR oder BWR)	107.3	28.2	0.263
74	EPRI BWR 1/4T	114.8	28.3	0.246
74	EPRI BWR 3/4T	98.1	26.5	0.271
74	EPRI Pwr 1/4T	108.2	28.0	0.259
74	EPRI Pwr 3/4T	79.2	23.6	0.298
74	LWR Kori Unit 3	75.6	21.6	0.286
74	OWR Omega West Reactor	73.0	17.9	0.246
74	EBR-II exp breeder reactor	141.9	36.5	0.257
74	Bor-60 Sevastianov	131.9	35.0	0.265
74	RTNS-II Fusion simulation sp	564.0	94.7	0.168
74	ITER FW	194.4	40.1	0.206
74	DEMO	150.2	32.9	0.219
74	IFMIF	355.7	66.4	0.187

W, arc-dpa—BCA:

Z	spectrum	standard NRT barn	modified barn	efficiency
74	APWR	106.5	27.8	0.261
74	KWO/PWR	94.6	23.8	0.252
74	TRIGA/TRADE	50.8	12.8	0.252
74	SNR-2	78.8	24.8	0.314
74	TTB (FRM)	63.6	16.5	0.259
74	Fission TETA=1.35 MeV	238.2	52.6	0.221
74	Fusion spectrum	150.2	35.6	0.237
74	14.8 MeV neutrons	574.6	115.8	0.202
74	(d,Be)n for 40 MeV deuterons	617.9	128.5	0.208
74	HFIR	56.1	14.7	0.263
74	PWR Robinson2	81.5	22.1	0.271
74	LWR (PWR oder BWR)	107.3	28.4	0.265
74	EPRI BWR 1/4T	114.8	28.7	0.250
74	EPRI BWR 3/4T	98.1	26.7	0.272
74	EPRI Pwr 1/4T	108.2	28.2	0.261
74	EPRI Pwr 3/4T	79.2	23.7	0.299
74	LWR Kori Unit 3	75.6	21.6	0.286
74	OWR Omega West Reactor	73.0	18.1	0.248
74	EBR-II exp breeder reactor	141.9	36.7	0.259

74	Bor-60 Sevastianov	131.9	35.1	0.266
74	RTNS-II Fusion simulation sp	564.0	113.9	0.202
74	ITER FW	194.4	44.0	0.226
74	DEMO	150.2	35.6	0.237
74	IFMIF	355.7	76.1	0.214

Part II

Relative difference (D) of the efficiencies presented in **Part I**

D= 100 × | η(arc-dpa-BCA) − η(arc-dpa)| /η (arc-dpa),

where

η(arc-dpa-BCA) = $\int \sigma_{\mathrm{arc-dpa-BCA}}(E)\varphi(E)dE / \int \sigma_{\mathrm{NRT}}(E)\varphi(E)dE$, and $\sigma_{\text{arc-dpa-BCA}}$ was calculated using results of arc-dpa-BCA simulations,

η(arc-dpa) = $\int \sigma_{\mathrm{arc-dpa}}(E)\varphi(E)dE / \int \sigma_{\mathrm{NRT}}(E)\varphi(E)dE$, and $\sigma_{\text{arc-dpa}}$ was calculated using the arc-dpa model

Z	spectrum	D (%)
4	APWR	4.0
4	KWO/PWR	4.1
4	TRIGA/TRADE	4.4
4	SNR-2	3.2
4	TTB (FRM)	4.1
4	Fission TETA=1.35 MeV	4.9
4	Fusion spectrum	3.8
4	14.8 MeV neutrons	5.8
4	HFIR	4.1
4	PWR Robinson2	3.8
4	LWR (PWR oder BWR)	3.9
4	EPRI BWR 1/4T	4.1
4	EPRI BWR 3/4T	3.9
4	EPRI Pwr 1/4T	4.0
4	EPRI Pwr 3/4T	3.6
4	LWR Kori Unit 3	3.7

4	OWR Omega West Reactor	4.3
4	EBR-II exp breeder reactor	4.0
4	Bor-60 Sevastianov	3.9
4	RTNS-II Fusion simulation sp	5.8
4	ITER FW	4.1
4	DEMO	3.8

13	APWR	0.67
13	KWO/PWR	0.67
13	TRIGA/TRADE	0.89
13	SNR-2	0.44
13	TTB (FRM)	0.89
13	Fission TETA=1.35 MeV	1.1
13	Fusion spectrum	2.2
13	14.8 MeV neutrons	4.7
13	(d,Be)n for 40 MeV deuterons	3.8
13	HFIR	0.89
13	PWR Robinson2	0.67
13	LWR (PWR oder BWR)	0.67
13	EPRI BWR 1/4T	0.89
13	EPRI BWR 3/4T	0.45
13	EPRI Pwr 1/4T	0.67
13	EPRI Pwr 3/4T	0.22
13	LWR Kori Unit 3	0.45
13	OWR Omega West Reactor	1.1
13	EBR-II exp breeder reactor	0.67
13	Bor-60 Sevastianov	0.45
13	RTNS-II Fusion simulation sp	4.7
13	ITER FW	2.7
13	DEMO	2.2
13	IFMIF	2.5

26	APWR	5.8
26	KWO/PWR	7.2
26	TRIGA/TRADE	8.0

26	SNR-2	3.2
26	TTB (FRM)	6.8
26	Fission TETA=1.35 MeV	9.0
26	Fusion spectrum	21.
26	14.8 MeV neutrons	33.
26	(d,Be)n for 40 MeV deuterons	31.
26	HFIR	7.1
26	PWR Robinson2	5.2
26	LWR (PWR oder BWR)	5.6
26	EPRI BWR 1/4T	7.8
26	EPRI BWR 3/4T	5.2
26	EPRI Pwr 1/4T	5.9
26	EPRI Pwr 3/4T	2.4
26	LWR Kori Unit 3	3.3
26	OWR Omega West Reactor	8.4
26	EBR-II exp breeder reactor	4.3
26	Bor-60 Sevastianov	4.0
26	RTNS-II Fusion simulation sp	33.
26	ITER FW	23.
26	DEMO	21.
26	IFMIF	22.

29	APWR	6.3
29	KWO/PWR	8.1
29	TRIGA/TRADE	9.8
29	SNR-2	2.4
29	TTB (FRM)	7.5
29	Fission TETA=1.35 MeV	11.
29	Fusion spectrum	32.
29	14.8 MeV neutrons	51.
29	(d,Be)n for 40 MeV deuterons	49.
29	HFIR	8.0
29	PWR Robinson2	5.2
29	LWR (PWR oder BWR)	5.8
29	EPRI BWR 1/4T	9.2
29	EPRI BWR 3/4T	5.8
29	EPRI Pwr 1/4T	6.4

29	EPRI Pwr 3/4T	2.5
29	LWR Kori Unit 3	3.1
29	OWR Omega West Reactor	9.8
29	EBR-II exp breeder reactor	4.8
29	Bor-60 Sevastianov	4.2
29	RTNS-II Fusion simulation sp	51.
29	ITER FW	35.
29	DEMO	32.
29	IFMIF	34.

74	APWR	0.38
74	KWO/PWR	0.80
74	TRIGA/TRADE	1.2
74	SNR-2	0.0
74	TTB (FRM)	0.78
74	Fission TETA=1.35 MeV	1.4
74	Fusion spectrum	8.2
74	14.8 MeV neutrons	20.
74	(d,Be)n for 40 MeV deuterons	27.
74	HFIR	0.77
74	PWR Robinson2	0.37
74	LWR (PWR oder BWR)	0.76
74	EPRI BWR 1/4T	1.6
74	EPRI BWR 3/4T	0.37
74	EPRI Pwr 1/4T	0.77
74	EPRI Pwr 3/4T	0.34
74	LWR Kori Unit 3	0.0
74	OWR Omega West Reactor	0.81
74	EBR-II exp breeder reactor	0.78
74	Bor-60 Sevastianov	0.38
74	RTNS-II Fusion simulation sp	20.
74	ITER FW	9.7
74	DEMO	8.2
74	IFMIF	14.

KIT Scientific Working Papers
ISSN 2194-1629

www.kit.edu